PNAS RESEARCH ARTICLE | ENGINEERING

Self-assembling paclitaxel-mediated stimulation of tumor-associated macrophages for postoperative treatment of glioblastoma

Feihu Wang[a,b,c,1], Qian Huang[d], Hao Su[a,b], Mingjiao Sun[a,b,c], Zeyu Wang[a], Ziqi Chen[a,b], Mengzhen Zheng[a,b], Rami W. Chakroun[a,b], Maya K. Monroe[a,b], Daiqing Chen[c], Zongyuan Wang[a,b], Noah Gorelick[e], Riccardo Serra[e], Han Wang[a,b], Yun Guan[d,f], Jung Soo Suk[a,c,f], Betty Tyler[e], Henry Brem[e,g,h,i], Justin Hanes[a,c,g,h,i], and Honggang Cui[a,b,c,i,j,2]

Edited by Alexander H. Stegh, Washington University in St Louis, St. Louis, MO; received March 15, 2022; accepted March 9, 2023 by Editorial Board Member Chad A. Mirkin

The unique cancer-associated immunosuppression in brain, combined with a paucity of infiltrating T cells, contributes to the low response rate and poor treatment outcomes of T cell-based immunotherapy for patients diagnosed with glioblastoma multiforme (GBM). Here, we report on a self-assembling paclitaxel (PTX) filament (PF) hydrogel that stimulates macrophage-mediated immune response for local treatment of recurrent glioblastoma. Our results suggest that aqueous PF solutions containing aCD47 can be directly deposited into the tumor resection cavity, enabling seamless hydrogel filling of the cavity and long-term release of both therapeutics. The PTX PFs elicit an immune-stimulating tumor microenvironment (TME) and thus sensitizes tumor to the aCD47-mediated blockade of the antiphagocytic "don't eat me" signal, which subsequently promotes tumor cell phagocytosis by macrophages and also triggers an antitumor T cell response. As adjuvant therapy after surgery, this aCD47/PF supramolecular hydrogel effectively suppresses primary brain tumor recurrence and prolongs overall survivals with minimal off-target side effects.

hydrogel | self-assembly | chemotherapy | immunotherpay | cancer

Glioblastoma multiforme (GBM) is the most aggressive neoplasm, with extremely high patient morbidity and mortality (1). Current clinical treatments for GBM focus on maximal safe surgical resection, implantation of Gliadel® Wafer (the only Food and Drug Administration (FDA)-approved carmustine implant) in the resection site (2, 3), adjuvant radiotherapy, and/or oral chemotherapy (2, 4, 5). Despite an initial modest therapeutic effect, infiltrating cancerous cells remain in the surrounding brain parenchyma following resection, leading to a need for improvement in therapies (4–6). While recent progress in immunotherapy has drastically improved clinical outcomes for patients with a few advanced cancers (7, 8), brain tumors continue to be a conspicuous exception to this trend, largely due to the unique immunosuppressive tumor environment in brain and insufficient infiltration of T cells into GBM (9). Even the most prominent immunotherapy approaches such as checkpoint inhibition, PD-1 and CTLA-4 blockade, and CAR-T cell therapies have shown limited benefit in GBM patients to date (10, 11). Of note, while we have previously demonstrated in a subcutaneous brain tumor model the enhanced immunotherapy efficacy by using camptothecin hydrogels to deliver a STING agonist (12) or aPD-1 (13), these systems do not perform as effectively in the orthotopic brain tumor model (*vide infra*), likely due to the pathological and biological differences associated with the chosen tumor models. Given that tumor-associated microglia/macrophages (TAMs) constitute 30 to 50% of brain tumor mass (14, 15), macrophage-directed immunotherapy has potential for improving the treatment of GBM (16, 17).

Macrophages are the main effectors of the innate immune response (18, 19). Recent studies have shown that cancer cells, including brain tumor, can evade innate immune surveillance via overexpression of the immune checkpoint CD47 (16, 20, 21). Through binding with and activating the macrophage surface receptor, signal regulatory protein α (SIRPα), CD47 acts as an antiphagocytic "don't eat me" signal to prevent macrophage phagocytosis of cancer cells (17, 22). Blocking CD47–SIRPα interaction with anti-CD47 antibody (aCD47) can promote tumor cell phagocytosis and, at the same time, trigger antitumor T cell immune response (23–25). While CD47 blockade has demonstrated therapeutic potential in clinical trials (26), aCD47 alone shows modest efficacy in suppressing tumor growth, even with multiple large doses[14]. While combination with chemotherapy or irradiation enables a more efficacious treatment of malignant brain tumors (25, 27, 28), systemic administration of CD47 antagonists and/or chemotherapeutics can

Significance

Combined use of protein drugs with small-molecule therapeutics can synergize their biological and pharmaceutical activities to improve treatment outcomes; however, their differences in molecular characteristics, such as size and water solubility, often lead to challenges in the development of effective drug codelivery systems. In this context, we convert paclitaxel (PTX), a small-molecule anticancer drug of poor water solubility, into a molecular hydrogelator that can be used for local delivery of aCD47, a hydrophilic macromolecular antibody. We show that this "drug-delivered-by-drug" strategy not only combines the distinct material properties of the two therapeutic agents for their long-acting local release, but also synergizes their biological properties to stimulate tumor-associated macrophages with concurrent T cell-mediated immune response for improved tumor treatment.

The authors declare no competing interest.

This article is a PNAS Direct Submission. A.H.S. is a guest editor invited by the Editorial Board.

[1]Present address: School of Biomedical Engineering, Shanghai Jiao Tong University, Shanghai 200240, PR China.

[2]To whom correspondence may be addressed. Email: hcui6@jhu.edu.

This article contains supporting information online at https://www.pnas.org/lookup/suppl/doi:10.1073/pnas.2204621120/-/DCSupplemental.

Published April 25, 2023.

cause severe side effects such as anemia and thrombocytopenia, thus incapable of unleashing the full potential of aCD47-based therapy (29–31). Given that surgical removal is still the primary option for glioma patients, we envision that direct delivery of aCD47 and a chemotherapeutic drug such as paclitaxel (PTX) into the resection cavity by a hydrogel scaffold could boost the immune activation and avoid off-target effects for GBM treatment (32–37).

PTX is one of the most efficacious and successful drugs in cancer chemotherapy and has been approved to treat a variety of cancer types (38). As a cell-cycle dependent, antimitotic drug, PTX selectively kills proliferating cells and, thus, represents a logical choice for local treatment of brain tumors. Recently, there has been mounting evidence to support that PTX can trigger infiltration of TAMs and induce enrichment of CD47 on cancer cells (39–41). These findings suggest that PTX has the ability to boost the immune response in a manner synergistic with CD47 blockade immunotherapy. We have recently shown that direct linkage of a chemotherapeutic agent onto a biologically active β-sheet-forming peptide transforms the drug into a supramolecular hydrogelator (42–45). The rapid solution-to-hydrogel phase transition of such self-assembling prodrug systems under physiological conditions allows for their deposition and retention in the resection cavity immediately after surgical removal of GBM (46–51). Based on these observations, we reason that such PTX-containing in situ-formed hydrogels can be exploited for localized delivery of immunotherapeutic agents (12, 13, 29), enabling a sustained, directed release of the combination therapy into the surrounding brain tissues to eradicate residual tumor cells.

In this context, we develop a PTX-bearing supramolecular hydrogel for site-specific delivery of aCD47 and PTX and demonstrate the promising results of this system for optimized combination of chemoimmunotherapy and enhanced inhibition of GBM recurrence (Fig. 1 *A* and *B*). Our findings reveal that the aCD47-loaded PTX prodrug hydrogelator forms a well-defined hydrogel upon infusion into the resection cavity. The hydrogel serves as a drug depot for localized, sustained release of both PTX and aCD47, eliciting an immune-stimulating tumor microenvironment (TME) and inducing macrophage phagocytosis of cancer cells.

Results

Characterization of aCD47/PF Supramolecular PTX Filament (PF) Hydrogel. To construct a bioresponsive hydrogel, a PTX prodrug hydrogelator (PTX–iRGD) was synthesized by chemically conjugating a PTX molecule to the iRGD peptide through a reducible 4-(pyridin-2-yl-disulfanyl)butyrate (buSS) linker using a previously reported method (52) (Fig. 1*A*). The detailed characterizations of PTX–iRGD can be found in *SI Appendix*, Figs. S1 and S2 *A* and *B*. iRGD was incorporated into the molecular design since it enhances penetration of tumor tissues by binding to neuropilin-1, leading to transcytosis. This rationally designed amphiphilic PTX prodrug spontaneously assembled into supramolecular PTX PF upon dissolution in water (Fig. 1*C* and *SI Appendix*, Fig. S2*C*). The addition of PBS or cell medium (Fig. 1*D* and Movie S1) to PTX PF aqueous solution induced rapid hydrogel formation due to charge screening between PTX PFs. The solution-to-hydrogel transition of PF was confirmed using rheological testing. Addition of PBS to the PF solution drastically increased the storage modulus (G′), indicating the formation of a supramolecular hydrogel (Fig. 1*E*). We hypothesized that the rapid solution-to-hydrogel transition of this PF hydrogelator may make it suitable to provide for localized controlled delivery of aCD47 monoclonal antibodies (mAbs). By simply mixing aqueous solutions of aCD47 and PF, followed by gelation induction by PBS (*SI Appendix*, Fig. S3*A*), aCD47 was loaded into the hydrogel (aCD47/PF). Moreover, confocal imaging revealed spatially uniform distribution of aCD47 throughout the hydrogel (*SI Appendix*, Fig. S3*B*).

The release of PTX–iRGD and aCD47 from aCD47/PF hydrogel was then investigated in PBS at 37°C. PTX–iRGD exhibited a linear release profile from aCD47/PF hydrogel, with ~35% PTX–iRGD released within 25 d. Approximately 30% of the encapsulated aCD47 was released over the first 5 d, followed by a gradually reduced release rate, with ~60% of aCD47 released over 25 d (Fig. 2*A*). These results display a typical release profile for encapsulated antibodies from a hydrogel matrix and unique zero-order release for PTX–iRGD, suggesting that the hydrogel serves as a depot for sustained release of therapeutic agents, and for controlled release of chemotherapeutic hydrogelator. The intracellularly rich reducing agent, glutathione (GSH), effectively liberates the parent PTX (*SI Appendix*, Fig. S4) through the reduction of the GSH-responsive buSS disulfide linker utilized in our PTX–iRGD prodrug design. In the presence of GSH, the liberation of free PTX from PTX–iRGD by disulfide reduction took place very quickly, with ~65% of parent PTX converted within 4 h (Fig. 2*B*), implying that PTX–iRGD could rapidly provide free PTX within cells (Fig. 2*C*). The PTX prodrug and its corresponding PF hydrogel achieved effective growth inhibition toward GL-261 tumor cells and tumor spheroids in vitro (*SI Appendix*, Fig. S5).

In Situ-Formed Hydrogel Enhanced Local Retention of aCD47 In Vivo and Reduced Side Effects. In vivo gelation was evaluated by subcutaneous injection of PF solution into mice. The injected PF transformed from a solution to a well-defined hydrogel within 10 min (Fig. 2*D*). This in situ-formed PF hydrogel exhibited gradual and nearly linear biodegradation by mass, with ~82% hydrogel weight loss within 45 d (Fig. 2 *D* and *E*). These results suggest that PF can serve as an in situ therapeutic depot at the target site for long-term release of therapeutics. Furthermore, to evaluate the in vivo retention behavior, Cy5.5-labeled aCD47 either in solution or encapsulated within PF solution was intratumorally injected into subcutaneous GL-261 tumor-bearing mice. Fluorescence signals in free aCD47-treated mice were detected in the tumor and major organs during the first 3 d (*SI Appendix*, Fig. S6), but the intensity dropped rapidly, with only ~5% left at the tumor sites after 8 d (Fig. 2 *F* and *G*). In sharp contrast, in the aCD47/PF-injected mice, almost all aCD47 was trapped within the tumors, with ~62% of aCD47 remaining throughout a large tumor area after 8 d (Fig. 2*G* and *SI Appendix*, Fig. S6). Confocal imaging of tumor sections further confirmed the PF hydrogel-induced local retention of aCD47, evident by strong fluorescence detected in aCD47/PF-treated tumors at 3 d following treatment (Fig. 2*H* and *SI Appendix*, Fig. S7). These results suggest that in situ-formed aCD47/PF hydrogel can significantly enhance drug retention within the target sites, and thus enable controlled release of aCD47 over a prolonged period of time.

Since the PF hydrogel can concentrate aCD47 at the desired site, we further investigated the safety of mice after intracranially injection of aCD47/PF solution. Ex vivo imaging demonstrated that aCD47 retained in the injection site in the brain and the in situ-formed hydrogel significantly prevented leakage of the aCD47 cargo (Fig. 2*I*). Although aCD47 was gradually released from the aCD47/PF hydrogel (Fig. 2*J*), fluorescent signals were hardly detectable in other major organs and blood over 45 d of investigation (*SI Appendix*, Fig. S8). Notably, body weight was not affected by intracranial injection of aCD47/PF

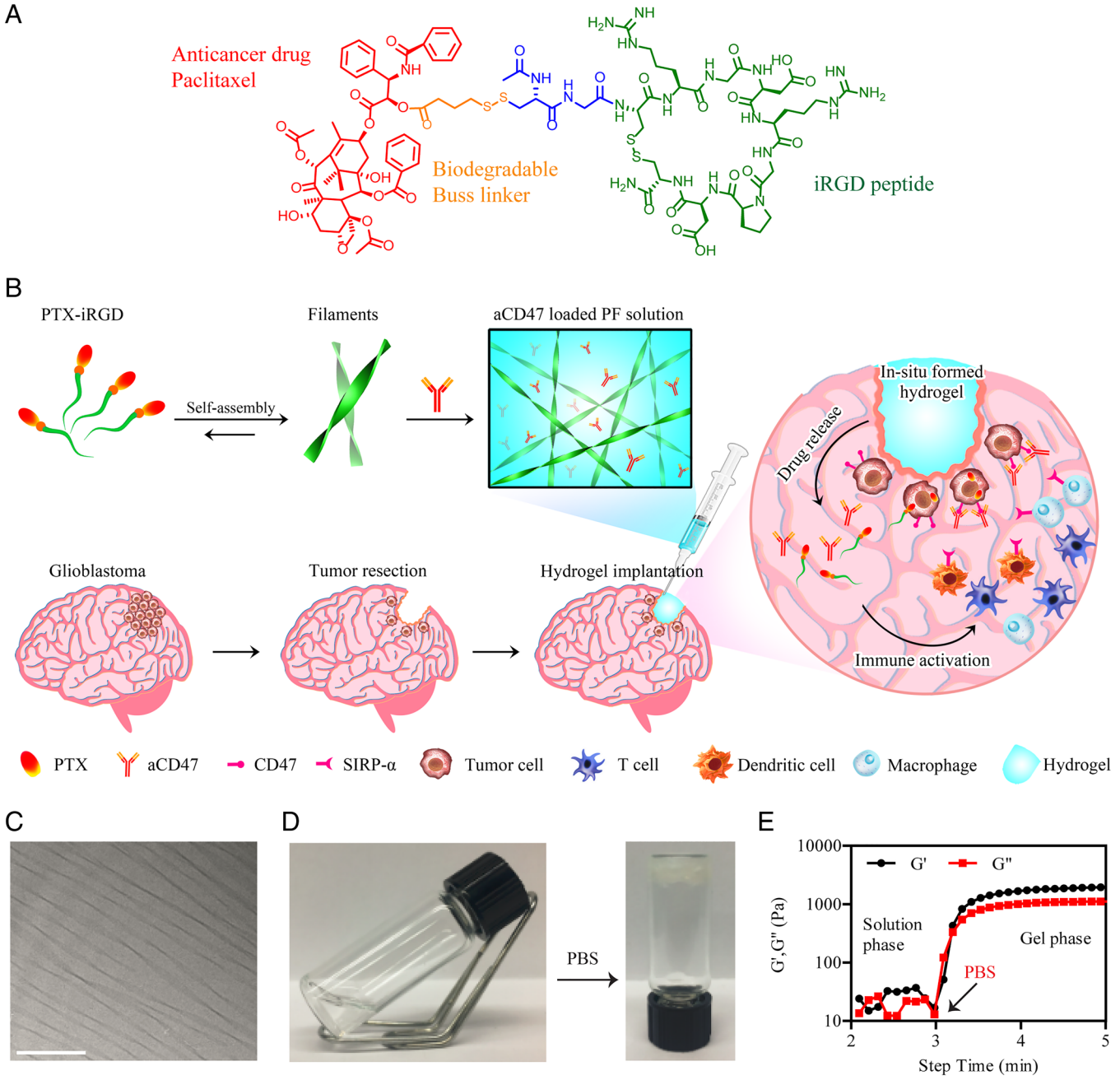

Fig. 1. Schematic illustration and characterization of self-assembling PTX hydrogelator. (*A*) Chemical structure of the designed PTX–iRGD prodrug amphiphile. (*B*) Schematic showing localized aCD47 delivery using a PTX PF hydrogel for the postresection treatment of glioblastoma. (*C*) Representative cryo-TEM of PTX–iRGD PFs. (Scale bar: 200 nm.) (*D*) Solution-to-hydrogel transition of PTX–iRGD PFs induced by addition of phosphate buffered saline (PBS). (*E*) Storage modulus (*G′*) and loss modulus (G″) of PF solution as a function of time. The rheological properties were assessed as the PF solution transitioned to a hydrogel upon addition of 10× PBS at 3 min.

(*SI Appendix*, Fig. S9*A*). Moreover, histological analysis of major organs, blood test, and serum biochemistry assay showed no notable difference between aCD47/PF-treated mice and healthy mice (*SI Appendix*, Figs. S9*B* and S10), suggesting that localized aCD47/PF did not cause obvious side effects.

aCD47/PF Elicits Regression of Orthotopic GBM. To evaluate therapeutic efficacy and investigate potential antitumor immune responses elicited by aCD47/PF hydrogel, we first utilized an orthotopic GL-261 brain tumor model in mice. For comparison, we designed DOCA–iRGD as a PTX-empty hydrogel (defined as EF gel) (*SI Appendix*, Fig. S11) for the local delivery of aCD47 (aCD47/EF). The hydrogelators EF, PF, aCD47/EF, and aCD47/PF were directly injected into established brain tumors on day 6 posttumor implantation. Tumor burden was monitored using bioluminescence signals and T2-weighted MRI (Fig. 3 *A* and *B*). Bioluminescence images and MR images displayed a rapid and aggressive growth of tumor mass in mice treated with "empty" EF hydrogel (Fig. 3 *A*–*C*) and demonstrated no statistical difference in survival compared to the untreated group (median survival, 21.5 vs. 22 d) (Fig. 3*D* and *SI Appendix*, Fig. S12). In contrast, PF- and aCD47/EF-treated mice exhibited relatively slow tumor growth (Fig. 3 *A* and *C*) and the tumor lesion was substantially reduced compared with the untreated group at day 20 posttumor implantation (Fig. 3*B*). On day 50, the tumor lesion can be barely observed, confirming the potential antiglioma effects of PF and

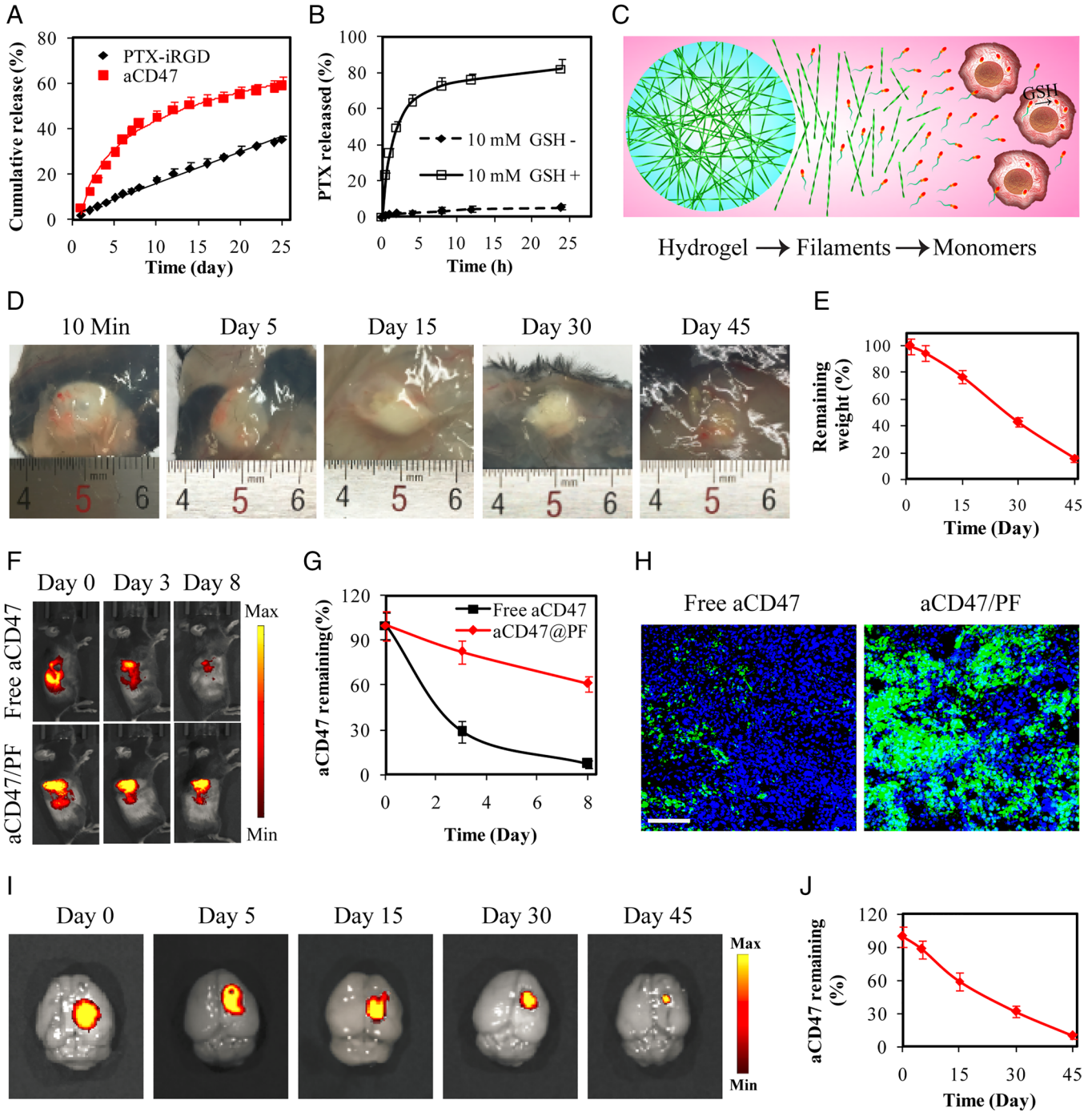

Fig. 2. Supramolecular PTX PF hydrogel scaffold extends local retention and release of aCD47 in situ. (*A*) Cumulative release profiles of PTX–iRGD and aCD47 from aCD47/PF supramolecular hydrogels. aCD47 was labeled with FITC. (*B*) Free PTX release profiles of 250 μM PTX–iRGD solution incubated with or without 10 mM GSH. (*C*) Schematic illustration of the proposed PTX release mechanism: hydrogel disruption, PTX PF dissociation followed by liberating the parent PTX in intracellular GSH reductive environment. (*D*) Images showing in vivo gelation and degradation of PTX–iRGD supramolecular hydrogels in C57BL/6 mice. (*E*) Quantification of the degradation profile of the PTX–iRGD supramolecular hydrogel. Data are given as mean ± SD (n = 3). (*F*) Fluorescent IVIS images showing the retention of aCD47 in the tumor at the indicated time points following intratumoral injection with free aCD47 or aCD47/PF solution, aCD47 was labeled with Cy5.5. (*G*) Quantification of the tumoral retention profile of aCD47. Data are given as mean ± SD (n = 3). (*H*) Fluorescence images of tumor sections from GL-261 tumor-bearing mice that were locally treated with free aCD47 or aCD47/PF on day 3. Green: FITC-labeled aCD47, Blue: DAPI-stained nuclei. (Scale bar: 200 μm.) (*I*) Ex vivo fluorescence images of brains intracranially injected with aCD47/PF confirmed the retention of aCD47 in the brain. aCD47 was labeled with Cy5.5. (*J*) Quantification of the retention profile of aCD47 in the brain. Data are given as mean ± SD (n = 3).

aCD47/EF (Fig. 3*B*). Twenty-five percent (median survival, 36 d) and 12.5% (median survival, 30 d) of the PF-treated and aCD47/EF-treated mice survived until the end of the study, respectively (Fig. 3*D* and *SI Appendix*, Fig. S12). Notably, aCD47/PF treatment dramatically inhibited brain tumor growth compared to the PF- and aCD47/EF-treated groups at 20 and 50 d (Fig. 3 *A*–*C*), with no tumor burden observed in long-term survival mice from MRI on day 50 (Fig. 3*B*). This combined treatment resulted in an extraordinary benefit in median survival (62 d), with 50% of aCD47/PF-treated mice surviving until the end of the study (Fig. 3*D* and *SI Appendix*, Fig. S12). For comparison, we also assessed the antitumor effect of aPD1/PF in this orthotopic brain tumor model (*SI Appendix*,

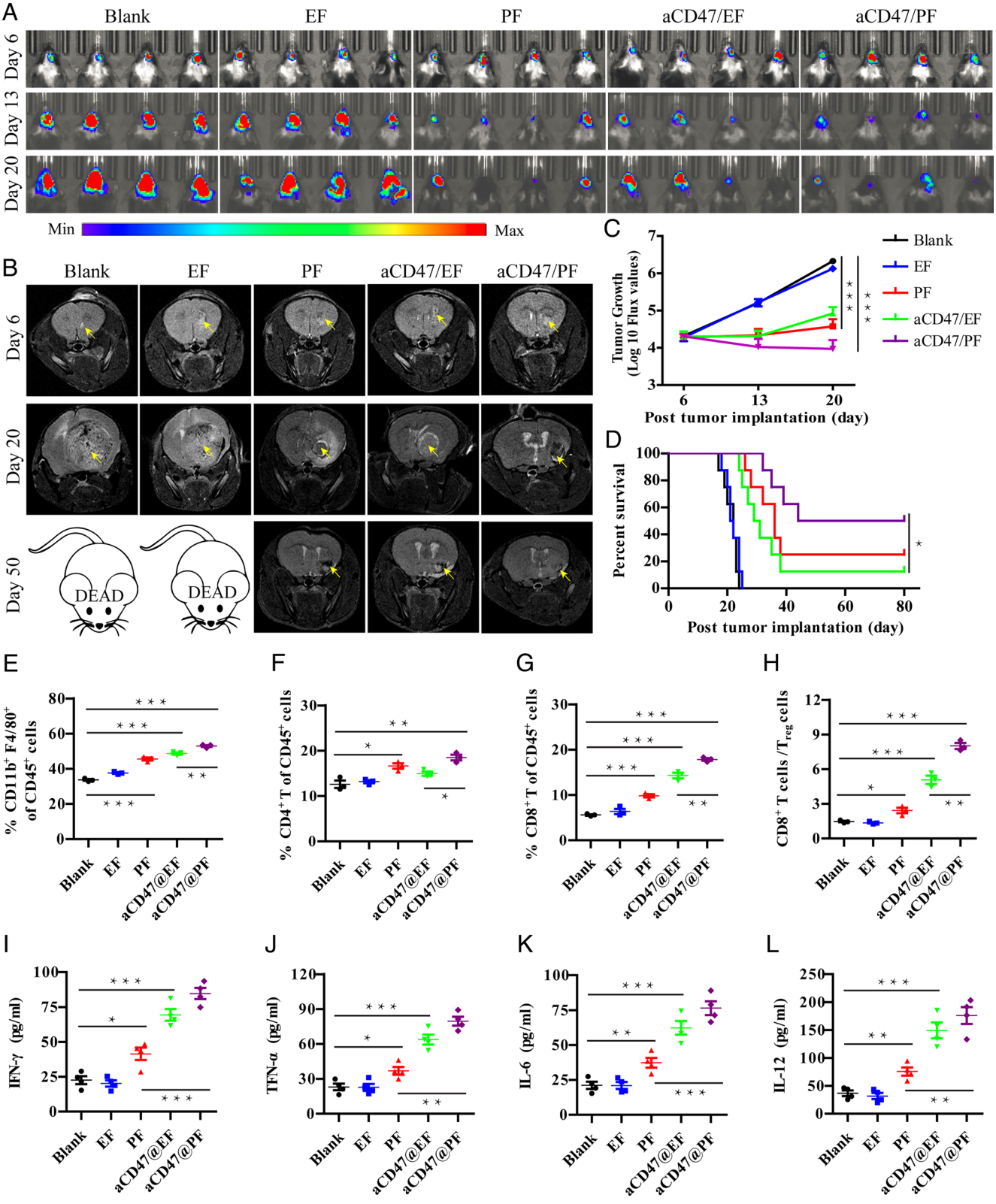

Fig. 3. aCD47/PF hydrogel elicits regression of GL-261 brain tumors. (*A*) In vivo bioluminescence images of GL-261 tumors in response to indicated treatments (n = 8 for each group). Four representative mice per treatment group are shown. (*B*) T2-weighted MR images of GL-261 brain tumors at day 6, 20, and 50 post injection. Lighter zones, indicated by yellow arrows, show tumor location within the brain. (*C*) Quantification of tumor growth from bioluminescence imaging of the GL-261 tumors in the indicated treatment groups. (*D*) Survival curves corresponding to indicated treatment groups. Statistical significance was calculated via the log-rank (Mantel–Cox) test. (*E*) Quantification of macrophage ($CD11b^+F4/80^+$), (*F*) $CD4^+$ T cell, and (*G*) $CD8^+$ T cell infiltration within the tumor following different treatments. (*H*) Ratios of the tumor-infiltrating $CD8^+$ T cells to T_{reg} cells in the indicated treatment groups. (*I*) Secretion levels of IFN-γ, (*J*) TNF-α, (*K*) IL-6, and (*L*) IL-12 at day 7 post different treatments. Statistical significance was calculated using a two-sided unpaired *t* test. Data are given as mean ± SD. $^*P \le 0.05$, $^{**}P \le 0.01$, $^{***}P \le 0.001$.

Fig. S13). Monotherapy with aPD1/EF led to a delay in brain tumor growth. The addition of aPD1 to PF hydrogel (aPD1/PF) does not seem to increase the benefit in tumor growth inhibition and prolong the median survival, when compared with those treated by PF alone. This is in sharp contrast to what was observed in the aCD47/PF-treated mice, suggesting a superior antitumor effect by the aCD47/PF hydrogel system.

Furthermore, residual tumors were collected, and the related immune cells were analyzed on day 10 posttreatment. The percentage of macrophages was significantly increased after PF treatment and aCD47 blockade (Fig. 3*E*). This tendency was further enhanced by the combined aCD47/PF treatment (60.9% in aCD47/PF group vs. 49.6% and 53.1% in PF and aCD47/EF groups, respectively) (Fig. 3*E*). Furthermore, we also observed that CD47 blockade enhanced infiltration of DCs in tumors (*SI Appendix*, Fig. S14*A*), leading to increased proportion of antigen-presenting $CD103^+$DCs, and $CD86^+$DCs (*SI Appendix*, Fig. S14 *B* and *C*), in consistent with previous studies on T cell-mediated antitumor immune response by aCD47-based therapy (25, 53). IFN-γ ELISpot responses in the splenocytes from the mice immunized with aCD47/EF and aCD47/PF were found to be significantly increased, implying robust in vivo antigen-specific T cell immune responses triggered by aCD47-loaded hydrogels (*SI Appendix*, Fig. S15 *A* and *B*). Subsequently, $CD8^+$ T (16.1% vs. 5.3% in Blank group) cell count significantly increased following aCD47/EF treatment (Fig. 3 *F* and *G* and *SI Appendix*, Fig. S16 *A* and *B*). Among all the treatment groups, aCD47/PF induced the highest percentages of $CD4^+$ and $CD8^+$ T cells. The proportion of $CD8^+$ T cells in the aCD47/PF-treated mice was 1.9-fold ($P \le 0.001$) and 1.3-fold ($P \le 0.05$) higher than those in the PF- and aCD47/EF-treated mice, respectively. The ratio of $CD8^+$ T cells to regulatory T cells (T_{reg}) was also significantly increased following aCD47/PF treatment (8.1% vs. 1.4% in Blank group) (Fig. 3*H*). Immune cell depletion experiments showed that $CD3^+$ T cells and $CD8^+$ T cells were critical to the observed aCD47/PF-induced antitumor effect (*SI Appendix*, Fig. S17). At the same time, macrophage depletion also led to significant reductions in overall survival rates. These results confirmed that aCD47/PF elicits tumor regression through priming $CD3^+$ T cells, $CD8^+$ T cells, and macrophages. Previous work by Weissman and coworkers suggests that macrophage phagocytosis of tumor cells mediated by CD47-specific blocking antibodies represents the major effector mechanism in orthotopic xenograft models (17, 24). Thus, while not directly shown in our studies, it is highly likely that the recruitment and activation of CD8+ T cells was mediated and further enhanced by the PTX/aCD47-activated macrophages. Moreover, cytokines such as IFN-γ, TNF-α, IL-6, and IL-12 were significantly secreted after aCD47-loaded hydrogel treatment (Fig. 3 *I–L* and *SI Appendix*, Fig. S18). From day 1 to day 7, the expression of these cytokines showed a time-dependent manner, and the increased secretion cytokines further validated the effective innate and adaptive immune responses elicited by aCD47/PF treatment. Together, these results suggest that aCD47/PF promotes a robust innate and adaptive antitumor immune response that dramatically inhibited brain tumor growth.

PF Hydrogel Elicits an Immune-Stimulating TME. To test whether PF has the potential to boost the local immune response in a manner synergistic with CD47 blockade immunotherapy, the related immune cells and tumor cells were investigated after treatment of PF hydrogel. As shown in Fig. 4 *E* and *F*, hydrogel had no obvious effects on tumor-infiltrating lymphocytesand tumor cells. In contrast, localized PF hydrogel treatment significantly increased the percentage of macrophages (50.1% vs. 34.8% in Blank group) in brain tumors (Fig. 4*A*). This result was supported by findings of an elevated interleukin-12 (IL-12) level in the TME which may be secreted from macrophages (Fig. 4*B*). PF treatment also induced infiltration of DCs in tumors (*SI Appendix*, Fig. S14*A*) and increased the proportion of immune effector $CD80^+$ dendritic cells (DCs), $CD103^+$DCs, and $CD86^+$DCs within the tumor (Fig. 4 *C–E*). These antigen-presenting DCs stimulated antigen-specific T cell immune responses (*SI Appendix*, Fig. S15). As a result, PF-treated tumors exhibited increased percentages of $CD4^+$ T (17.5% vs. 13.3% in Blank group) and $CD8^+$ T (10.6% vs. 5.6% in Blank group) cells compared to control groups (Fig. 4 *F* and *G*). This is consistent with previous reports that PTX can elicit DC-mediated phagocytosis and subsequent activation of cytotoxic T lymphocytes (54, 55). The increased secretion of interferon-γ (IFN-γ) and tumor necrosis factor-α (TNF-α) further suggests an effective immune response elicited by PF treatment (Fig. 4 *H* and *I*). Although $Foxp3^+CD4^+$ T cells were slightly increased (Fig. 4*J*), we observed a significant reduction of myeloid-derived suppressor cells (MDSC, $CD11b^+Gr\text{-}1^+$) (17.1% vs. 31.4% in Blank group) in brain tumors treated with PF (Fig. 4*K*). As measured by flow cytometry, immune checkpoint CD47 is highly expressed on the surface of GL-261 brain cancer cells (Fig. 4*L*). Compared to control or EF treatment, PF further enhanced the enrichment of CD47 on GL-261 cells (Fig. 4*M*). Collectively, these findings demonstrate that PF hydrogel promotes an immune-stimulating TME in GL-261 brain tumors in mice.

aCD47/PF Prevents Orthotopic GBM Recurrence after Surgery. Given that surgical resection is the current standard of care for GBM, we developed a brain tumor resection model to further test the aCD47/PF hydrogel as potential GBM therapy. At day 8 after tumor cell inoculation, the tumor developed to adequate size with small tumor islands around the primary tumor mass evident by MRI (Fig. 5*A*). Based on findings in our pilot study (*SI Appendix*, Fig. S19), day 8 was selected to be the optimal time for surgery in the GBM resection model (Fig. 5 *B*, *i–iii*). Resection did not induce neurological impairment or any notable side effects. To validate the model following surgery, mice were immediately killed to confirm the efficiency of resection. The resection cavity could be clearly observed from hematoxylin and eosin H&E-stained brain sections (Fig. 5*C*). The primary tumor mass was almost completely removed, with small tumor deposits remaining in the normal brain parenchyma around the surgical cavity. The extent of tumor resection was quantitatively assessed by bioluminescence analysis, which showed that ~95% of GBM mass was removed by the surgery (Fig. 5*D*). These results demonstrate the accurate surgical resection of intracranial GBM in mice, which closely mimics the maximal resection procedure adopted for human GBM patients. Although survival analysis showed that surgical resection extended survival time (median survival, 28.5 d resected vs. 22 d untreated), the benefit was modest and all mice succumbed to tumor recurrence (Fig. 5*E*).

To test the inhibition of tumor recurrence by aCD47/PF hydrogel, aCD47/PF solution was intraoperatively infused into the resection cavity (Fig. 5 *B*, *iv*). In the presence of biological fluid, aCD47/PF gelation was formed rapidly within the resection cavity. This in situ hydrogel seamlessly filled up the cavity left by tumor resection, thereby serving as a reservoir for long-term, localized release of therapeutic agents. Bioluminescence imaging confirmed that all mice developed a well-demarcated tumor at day 8 postinoculation. The luminescence intensity from brain tumors was significantly reduced after surgical tumor removal (day 9) (Fig. 5*F*). Similar to the resected mice in the control group, tumor recurrence and growth occurred aggressively in mice that underwent resection followed by EF treatment (Fig. 5 *F–H*). All

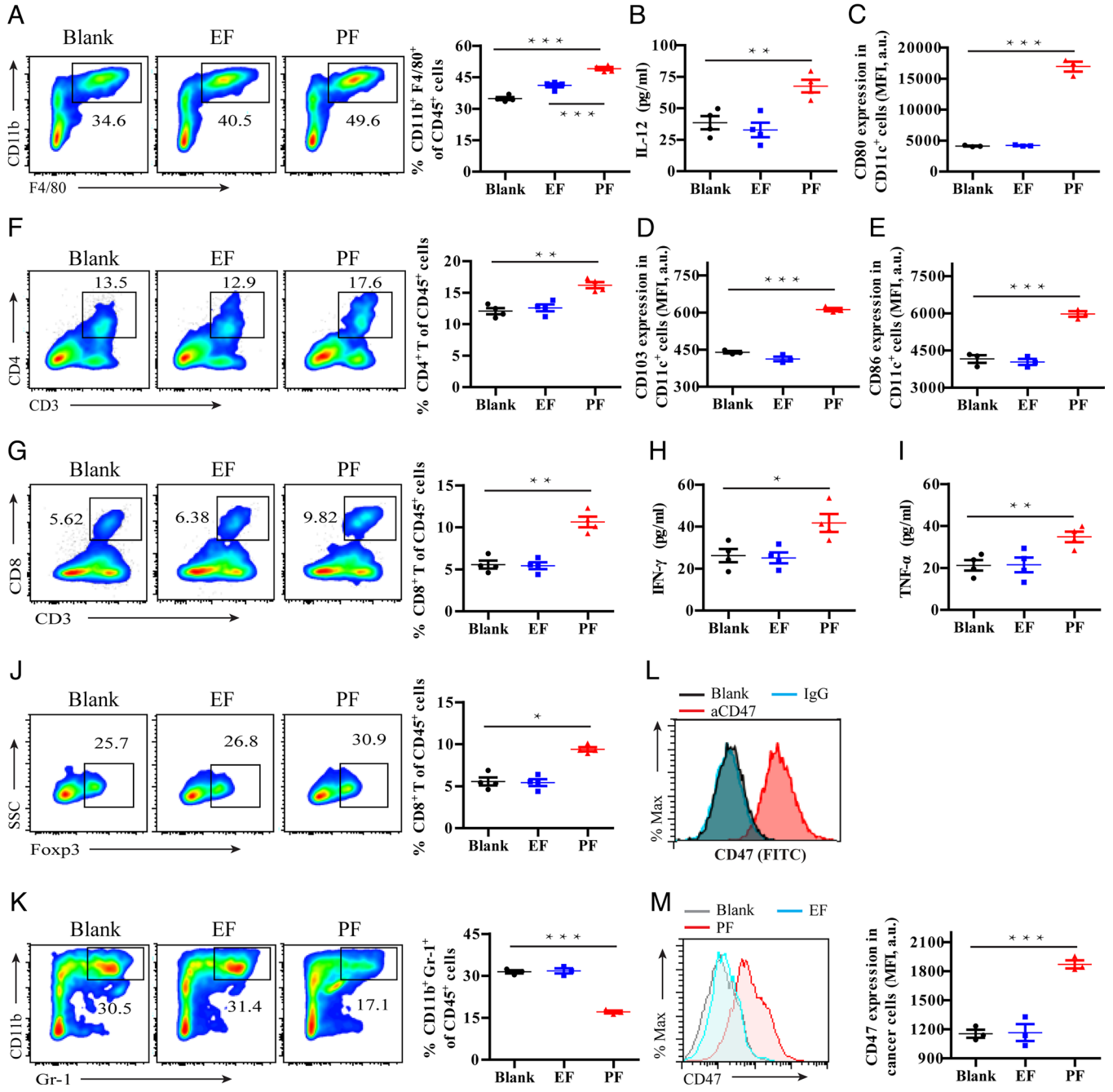

Fig. 4. PF hydrogel triggers a robust antitumor immunity. (*A*) Representative images and corresponding quantification of flow cytometric analyses of macrophages ($CD11b^+F4/80^+$) within brain tumors in the indicated treatment groups. (*B*) Secretion levels of IL-12 in the indicated treatment groups. (*C*) Quantification of $CD80^+$, (*D*) $CD103^+$, and (*E*) $CD86^+$ DCs in the indicated treatment groups. (*F*) Representative images and corresponding quantification of flow cytometric analyses of $CD4^+$ T cell infiltration within the tumor in the indicated treatment groups. (*G*) Representative images and corresponding quantification of flow cytometric analyses of $CD8^+$ T cell infiltration within the tumor in the indicated treatment groups. (*H*) Secretion levels of IFN-γ and (*I*) TNF-α in the indicated treatment groups. (*J*) Representative images and relative quantification of flow cytometric analyses of $Foxp3^+$ cells gating on $CD4^+$ T cells. (*K*) Representative images and relative quantification of flow cytometric analyses of MDSC ($CD11b^+Gr\text{-}1^+$) gating on $CD45^+$ cells. (*L*) Representative flow cytometric analysis of surface expression of CD47 on GL-261 brain tumor cells. (*M*) Representative images and relative quantification of flow cytometric analysis of CD47 expression in GL-261 brain tumors after different treatments. Statistical significance was calculated using a two-sided unpaired *t* test. Data are given as mean ± SD (n = 3). $^*P \le 0.05$, $^{**}P \le 0.01$, $^{***}P \le 0.001$.

EF-treated mice died within 36 d and showed no difference in survival time, as compared with the mice that received tumor resection only (median survival, 29.5 vs. 28.5 d) (Fig. 5*I* and *SI Appendix*, Fig. S20*A*). Single-drug treatment with PF or aCD47/EF significantly reduced tumor recurrence, with tumor burdens sharply decreased compared to those of untreated resected mice (Fig. 5 *F*–*H*). Both treatments prolonged the median survival time (63 and 39 d, respectively) and improved survival rate of 50% and 25%, respectively (Fig. 5*I* and *SI Appendix*, Fig. S20*A*). Strikingly, no tumor growth was found, by either IVIS or MRI in brain tissues of mice treated with combination aCD47/PF therapy (Fig. 5 *F*–*H*). Resection surgery plus aCD47/PF treatment eliminated tumor recurrence, leading to 100% survival (Fig. 5*I*), in contrast to aCD47/PF-treated mice without resection (*SI Appendix*, Fig. S20*B*). Collectively, these data suggest that site-specific aCD47/PF hydrogel implantation as an adjunct therapy to surgical resection shows promise as an effective treatment approach for GBM.

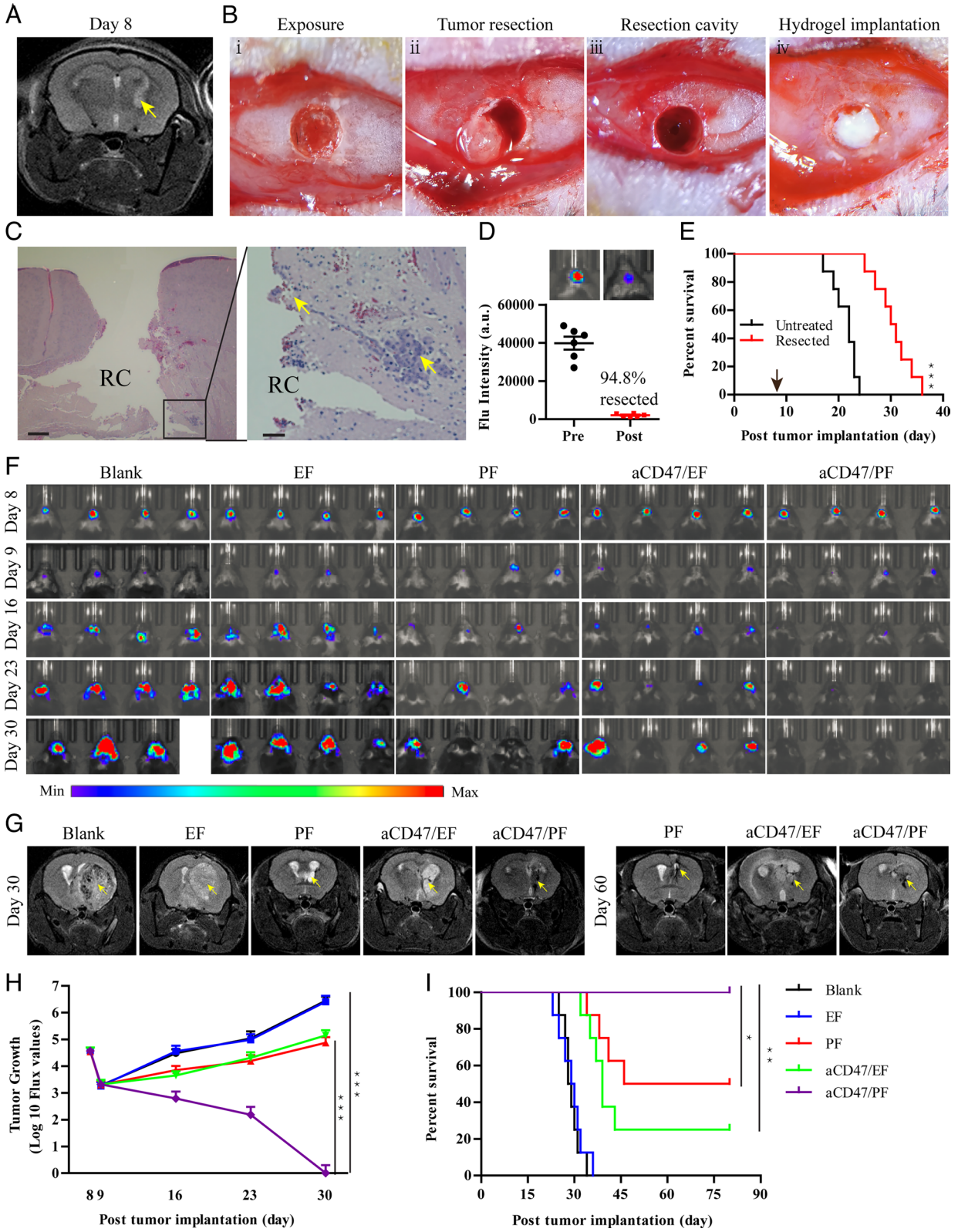

Fig. 5. aCD47/PF hydrogel inhibits brain tumor recurrence after resection. (*A*) T2-weighted images of GL-261 brain tumors obtained through MRI showing tumor growth at day 8. Lighter zones indicated by yellow arrows show the tumor location within the brain. (*B*) Procedure of surgical tumor resection from the GL-261 tumor-bearing mice and hydrogel implantation. (*C*) H&E staining of the brain sections collected from the GL-261-bearing mice immediately following surgical tumor removal. RC indicates the resection cavity. (Scale bar: *Left*, 500 μm; *Right*, 100 μm.) (*D*) Representative images and quantitative analysis showing the extent of surgical resection using bioluminescence imaging. (*E*) Survival curves of GL-261 brain tumor-bearing mice with or without surgical resection (n = 8). Arrow indicates the time of the surgery. Statistical significance was determined via the log-rank (Mantel–Cox) test. (*F*) In vivo bioluminescence images of surgically treated GL-261 tumors in response to indicated treatments (n = 8 for each group). Four representative mice per treatment group are shown. (*G*) T2-weighted MR images of surgically treated GL-261 brain tumors at day 30 and 60 post tumor implantation. (*H*) Quantification of bioluminescence imaging of the surgically treated GL-261 tumors in the indicated treatment groups. (*I*) Survival curves of surgically treated GL-261 brain tumor-bearing mice corresponding to indicated treatments. Statistical significance was calculated via the log-rank (Mantel–Cox) test. Data are given as mean ± SD. $*P \le 0.05$, $**P \le 0.01$, $***P \le 0.001$.

aCD47/PF Elicits Durable Antitumor Immune Response. Mice that survived following an initial treatment, called long-term survivors, were rechallenged with GL-261 cells to assess whether localized aCD47/PF elicited a memory immune response (Fig. 6*A*). As illustrated by the bioluminescence imaging, naïve mice developed progressive and large tumors, which led to 100% fatality within 24 d after tumor cell inoculation (Fig. 6 *B*–*D*). In contrast, although some mice exhibited initial tumor growth in the first few days, no bioluminescence signal was detected in the PF, aCD47/EF, and aCD47/PF groups on day 20 postrechallenge (Fig. 6 *B* and *C*). These results unravel effective inhibition of tumor growth and a robust memory immune response in the surviving mice. Indeed, in the rechallenged long-term surviving mice, flow cytometry analyses of immune cells in the spleen showed increased percentages of $CD4^+CD44^{high}CD62L^{low}$ T effector memory cells ($CD4^+$ $T_{em)}$ and $CD8^+CD44^{high}CD62L^{low}$ T effector memory cells ($CD8^+$ $T_{em)}$ (Fig. 6 *E* and *F*). Notably, aCD47/PF-treated mice possessed a much higher survival rate and larger proportions of $CD4^+$ (29.9% vs. 17.6%) and $CD8^+$ T_{em} (16.9% vs. 7.3%), as compared with Blank group (Fig. 6 *D*–*F*). These results strongly substantiate that a robust and durable antitumor memory immune response was established by a single localized aCD47/PF hydrogel treatment.

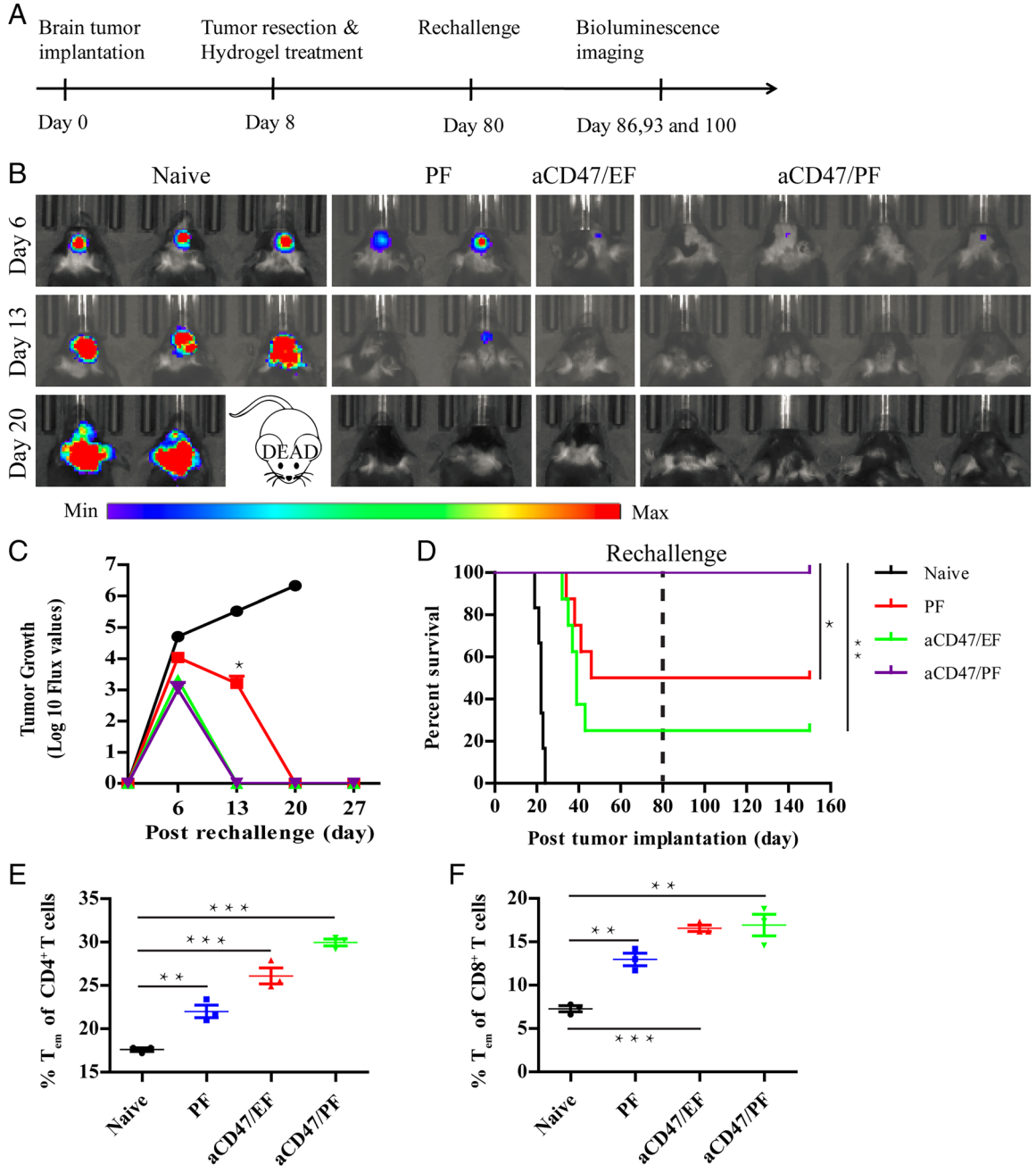

Fig. 6. aCD47/PF hydrogel induces durable antitumor immune response. (*A*) The experimental scheme showing the treatment schedule as well as the timing of the rechallenge. (*B*) In vivo bioluminescence images of the GL-261 tumors of naïve and rechallenged mice taken on days 6, 13, and 20 post tumoral rechallenge. (*C*) Quantification of bioluminescence imaging of naïve and rechallenged mice in the indicated treatment groups. (*D*) Survival curves for naive and rechallenged mice corresponding to the indicated treatment groups. Statistical significance was determined via the log-rank (Mantel–Cox) test. (*E*) The percentage of $CD4^+$ T_{em} cells and (*F*) $CD8^+$ T_{em} cells in splenocytes of the naïve and rechallenged mice. Statistical significance was determined using a two-sided unpaired *t* test. Data are given as mean ± SD (n = 3). $^*P \le 0.05$, $^{**}P \le 0.01$, $^{***}P \le 0.001$.

Conclusion

Since its approval by the FDA in 1995, Gliadel® Wafer remains as the first and only local chemotherapeutic treatment of GBM. The clinical successes of Gliadel® Wafer clearly suggests that the combination of surgical resection with local drug delivery systems offers an effective treatment strategy to prolong the survival of brain tumor patients. By leveraging the recent advancements in cancer immunotherapy, we developed a self-assembling prodrug hydrogel system to deliver both PTX and aCD47 following GBM resection as a therapeutic approach for this devastating disease. We demonstrated that a well-defined aCD47/PF hydrogel was formed rapidly after deposition of aCD47-containing PF solution into the resection cavity. This in situ-formed PTX PFs hydrogel seamlessly filled the cavity left by GBM resection, serving as a reservoir for long-term, localized release of both PTX and aCD47 to residual tumor tissue. Our in vivo results revealed that PF hydrogel elicited an immune-stimulating TME with enhanced infiltration of TAMs, DCs, and $CD8^+$ T cells and enrichment of CD47 on cancer cells. Our work suggests that PTX acted in concert with the locally released aCD47 to stimulate tumor-associated macrophages with subsequent/concurrent T cell-mediated antitumor immune responses. As such, this innovative chemoimmunotherapy aCD47/PF hydrogel significantly suppressed tumor recurrence following postsurgical removal of GBM and demonstrated a striking 100% survival rate. Moreover, the local administration of the hydrogel generated robust effector T cell memory, thereby also preventing tumor recurrence. It is noteworthy that this self-supporting hydrogel contains only the PTX prodrug, thus avoiding any potential toxicities from additional excipient materials. More importantly, the in situ-formed hydrogel increases the therapeutic concentration at the target site while preventing leakage of the drugs into blood stream and major organs, so as to reduce off-target side effects. Collectively, these results suggest that site-specific aCD47/PF hydrogel injection following surgical resection is a highly promising and clinically relevant chemoimmunotherapy strategy for the treatment of recurrent GBM. Despite these highly encouraging results, it should be noted that our work has been tested only in one clonotypic GBM model. Considering that GL-261 model is moderately immunogenic relative to human GBM, additional animal models that can more accurately represent the immune phenotype characteristics of GBM shall be used to further validate the clinical potential of the reported PTX/aCD47 hydrogel.

Materials and Methods

Materials, Cell Lines, and Animals. All amino acids and Rink Amide MBHA Resin were purchased from AAPPTEC (Louisville, KY). Anti-CD47 antibody (cat. no. 127519) was obtained from BioLegend. All other reagents and solvents were purchased from Sigma-Aldrich. GL-261-luc cells were obtained from M. Lim at The Johns Hopkins University. The cells were cultured in DMEM (Gibco, Invitrogen) supplemented with 100 μg/mL G418 (Invitrogen). Eight-to-ten-week-old female C57BL/6 mice were purchased from Charles River. Animal experiments were carried out following the animal protocol approved by the Animal Care and Welfare Committee at The Johns Hopkins University.

Synthesis of PTX–iRGD. Through the standard Fmoc-solid-phase technique, an AAPPTEC Focus XC synthesizer was used to synthesize the peptide C_2K -cyl[CRGDRGPDC]. RP-HPLC and MALDI-TOF MS were used to purify and analyze the peptide, respectively. PTX was chemically modified to PTX–buss–Pyr as previously reported (42, 56). Then, PTX–buss–Pyr and purified peptide were mixed at a molar ratio of 1:1.5 (PTX–buss–Pyr/peptide) in 5 mL N_2-purged DMSO and allowed to react for 3 d. The crude reaction solution was purified by RP-HPLC, and then the product was confirmed by ESI MS and lyophilized to obtain PTX–iRGD as a white powder.

Preparation of aCD47/PF Hydrogel. PF hydrogel formation was tested by adding 15 μL 10× PBS to 150 μL 17.5 mM PF solution. For preparation of aCD47-loaded PF hydrogel (aCD47/PF), aCD47 (50 μg) was added to the PF solution (200 μg PTX). After vortexing, 10× PBS was added to the mixture to induce the formation of aCD47/PF hydrogel. The inverted-vial method was then performed to test sol-to-gel transition. aCD47 dispersion in the hydrogel was further characterized using confocal microscopy (Zeiss LSM 510). For in vivo application, aCD47 and PF mixture solution was loaded into a syringe and directly injected into the target sites to form a gel in situ.

Hydrogel Degradation Study. A volume of 100 μL 17.5 mM PF solution was subcutaneously injected into C57BL/6 mice. At predetermined time points, the mice were killed and the remaining hydrogel in each mouse was photographed. Hydrogel weights were determined by detecting the amount of PTX–iRGD within the hydrogel.

Drug Release from aCD47/PF Hydrogel. The in vitro release study was performed at 37 °C in PBS with 10% FBS. The released PTX–iRGD was quantified by HPLC, whereas released aCD47 (labeled with Cy3) was analyzed using a fluorescence spectrophotometer. To evaluate the in vivo release of aCD47, free aCD47 or aCD47/PF solutions were injected into the subcutaneous GL-261-luc tumors, which were generated by inoculating 2.5×10^6 cells on the right flanks of female C57BL/6 mice for 10 d. At predetermined time points, fluorescence imaging of Cy5.5–aCD47 was completed using an IVIS Spectrum imaging system (Perkin Elmer). Harvested tumors were also cut into sections, stained with DAPI, and imaged using a confocal microscope (Zeiss LSM 510). Furthermore, to evaluate the release of aCD47 in the brain, the mice were intracranially implanted with aCD47/PF hydrogel. Briefly, the mice were anesthetized and stereotactically injected with 10 μL aCD47/PF solution using a 25-μL Hamilton syringe fitted with a 26 G needle. The injection coordinates were 2.5 mm lateral, 0.5 mm anterior to bregma, and 2.5 mm deep from the outer border of the cranium. At predetermined time points, brains were taken out and fluorescence imaging of Cy5.5–aCD47 was completed using an IVIS Spectrum imaging system (Perkin Elmer).

Glioblastoma Tumor Model and Local Treatment. An orthotopic glioblastoma tumor model was developed by intracranial implant of GL-261 glioma cells (57, 58). Mice were anesthetized by intraperitoneal injection of ketamine/xylazine. Once prepped for surgery, the mice were positioned on a stereotactic frame and a 5-mm-long midline scalp incision was made. A burr hole was drilled at the right cranial hemisphere, 2.5 mm lateral and 0.5 mm anterior to bregma. Then, 1×10^5 GL-261-luc cells were implanted at a depth of 2.5 mm from the dura. The skin was closed with tissue glue. On day 6 after inoculation, brain tumor-bearing mice were randomly assigned to five groups (n = 8). The cranium was reopened and 10 μL of treatment solutions was injected in the previous burr hole using a 25-μL Hamilton syringe fitted with a 26 G needle. The treatment groups were as follows: saline, drug-free DOCA–iRGD PTX PF solution (EF), PTX–iRGD PTX PF solution, aCD47-loaded DOCA–iRGD PTX PF solution (aCD47/EF), or aCD47-loaded PTX–iRGD PTX PF solution (aCD47/PF). Administered drug doses were 50 μg aCD47 and 150 μg PTX per mouse. Body weights and behavior of the mice were monitored daily postoperation and treatment. The mice were euthanized according to IACUC-approved guidelines when body weight loss surpassed 20%.

Orthotopic GBM Tumor Resection Model and Treatment. At day 8 posttumor implantation, well-established tumors had formed and the tumor resection was performed using method similar to those previously reported (48, 57). Briefly, mice were anesthetized, then immobilized on a stereotactic frame, and a midline incision was made in the skin above the cranium to expose the previous burr hole. Under a dissecting surgical microscope, the brain tumor was surgically resected using a biopsy punch. Tumor tissue and blood were aspirated using a vacuum pump. Then, 10 μL of formulation solution was injected into the resection cavity using a 25-μL Hamilton syringe fitted with a 26 G needle. Finally, the wound was closed with tissue glue. The treatment groups were as follows (n = 8 for each group): saline, EF, PF, aCD47/EF, or aCD47/PF. The dosages of administered drugs were 50 μg aCD47 and 150 μg PTX per mouse.

Mice were considered long-term survivors if no tumor was detected 80 d post-tumor implantation. Long-term survivors from all treatment groups were rechallenged at day 80 with 2×10^5 GL-261-luc cells in the contralateral hemisphere to

develop new tumors. Naïve mice were intracranially implanted as controls. Tumor growth was checked weekly using IVIS imaging. Body weight and behavior of the mice were also monitored postsurgical resection and treatment. The mice were killed when body weight loss surpassed 20%.

Brain Tumor Growth Monitoring. Tumor growth in the brain was monitored by bioluminescence imaging using an IVIS Spectrum Imaging System. Bioluminescence images were analyzed using Living Image software (Perkin Elmer). The location and size of brain tumors were also tracked by MRI using a horizontal bore 4.7 T Biospec animal imager (Bruker BioSpin). T2 -weighted images were acquired in the horizontal plane at predetermined time points. Additionally, to examine the pattern of tumor growth, mice were killed at different days and specimens of the brain were harvested, fixed, and stained with H&E. The H&E-stained brain slides were then imaged using an optical microscope.

Safety Study of Hydrogel in Healthy Mice. Ten-week-old healthy female C57BL/6 mice were anesthetized, a burr hole was made as described above, and then 10 μL aCD47/EF solution was injected in the burr hole using a 25-μL Hamilton syringe fitted with a 26 G needle. At predetermined time points, blood samples were harvested and complete blood cell count and serum biochemistry were determined. After 1 mo, the mice were killed, the brain and other major organs were harvested, fixed, and stained with H&E. The slides were then imaged using an optical microscope.

Flow Cytometry. Tumors collected from mice were digested with 1 mg/mL collagenase digestion buffer (Type IV, Gibco) to get single-cell suspensions. The cells were then stained with fluorescence-labeled antibodies following the manufacturer's instructions. Flow cytometry was performed using a FACSCanto II instrument (BD Biosciences) and analyzed by FlowJo software (Tree Star). Antibodies against CD45 (30-F11), CD11b (ICRF44), F4/80 (BM8), CD3 (17A2), CD4 (RM4-5), CD8 (53-6.7), Foxp3 (FJK-16s), Gr-1 (RB6-8C5), CD80 (16-10A1), CD86 (GL-1), CD103 (2E7), CD44 (IM7), and CD62L (MEL-14) were purchased from BioLegend or eBioscience. To detect the expression of CD47 on the tumor cells, cells were stained with fluorescein isothiocyanate (FITC)-labeled anti-CD47 antibody (miap301) and measured using flow cytometer.

Cytokine Analysis. Blood samples were collected from mice on day 1, 3, and 7 posttreatments. Serum levels of IL-6, IL-12, IFN-γ, and TNF-α were measured using enzyme-linked immunosorbent assay (ELISA) kits according to the manufacturer's instructions.

Statistical Analysis. All results were presented as means ± SD. The two-tailed unpaired *t* test was used to determine statistical significance between two treatment groups and ANOVA was used for multiple comparisons. Survival was plotted using a Kaplan–Meier curve and assessed by a log-rank (Mantel–Cox) test. Statistical analysis was performed using GraphPad Prism software 5. $*P \leq 0.05$, $**P \leq 0.01$, $***P \leq 0.001$.

Data, Materials, and Software Availability. All study data are included in the article and/or *SI Appendix*. Some study data available (Necessary materials are available from the corresponding author on reasonable request).

ACKNOWLEDGMENTS. The work is supported by Johns Hopkins University Discovery Award. Q.H. and Y.G.'s efforts were supported by NIH (Bethesda, Maryland, USA) grants NS110598 (Y.G.) and NS117761 (Y.G.). We thank Dr. M. Lim from Johns Hopkins University School of Medicine for sharing the GL-261-luc cells. We also thank Dr. D. Q. Xu for her help in flow cytometry studies and data analysis.

Author affiliations: [a]Department of Chemical and Biomolecular Engineering, Whiting School of Engineering, The Johns Hopkins University, Baltimore, MD 21218; [b]Whiting School of Engineering, Institute for NanoBiotechnology, The Johns Hopkins University, Baltimore, MD 21218; [c]Center for Nanomedicine, Wilmer Eye Institute, School of Medicine, The Johns Hopkins University, Baltimore, MD 21231; [d]Department of Anesthesiology and Critical Care Medicine, School of Medicine, The Johns Hopkins University, Baltimore, MD 21205; [e]Department of Neurosurgery, School of Medicine, The Johns Hopkins University, Baltimore, MD 21231; [f]Department of Neurological Surgery, School of Medicine, The Johns Hopkins University, Baltimore, MD 21231; [g]Department of Ophthalmology, School of Medicine, The Johns Hopkins University, Baltimore, MD 21231; [h]Department of Biomedical Engineering, School of Medicine, The Johns Hopkins University, Baltimore, MD 21231; [i]Department of Oncology and the Sidney Kimmel Comprehensive Cancer Center, School of Medicine, The Johns Hopkins University, Baltimore, MD 21231; and [j]Department of Materials Science and Engineering, Whiting School of Engineering, The Johns Hopkins University, Baltimore, MD 21218

Author contributions: F.W. and H.C. designed research; F.W., Q.H., H.S., M.S., Z.W., Z.C., M.Z., R.W.C., D.C., Z.W., N.G., R.S., H.W., and H.C. performed research; F.W., Q.H., J.H., and H.C. analyzed data; and F.W., M.K.M., Y.G., J.S.S., B.T., H.B., J.H., and H.C. wrote the paper.

1. M. S. Lesniak, H. Brem, Targeted therapy for brain tumours. *Nat. Rev. Drug. Discov.* **3**, 499–508 (2004).
2. M. J. McGirt *et al.*, Gliadel (BCNU) wafer plus concomitant temozolomide therapy after primary resection of glioblastoma multiforme. *J. Neurosurg.* **110**, 583–588 (2009).
3. F. J. Attenello *et al.*, Use of Gliadel (BCNU) wafer in the surgical treatment of malignant glioma: A 10-year institutional experience. *Ann. Surg. Oncol.* **15**, 2887–2893 (2008).
4. S. A. Chowdhary, T. Ryken, H. B. Newton, Survival outcomes and safety of carmustine wafers in the treatment of high-grade gliomas: A meta-analysis. *J. Neurooncol.* **122**, 367–382 (2015).
5. R. Stupp *et al.*, Effects of radiotherapy with concomitant and adjuvant temozolomide versus radiotherapy alone on survival in glioblastoma in a randomised phase III study: 5-year analysis of the EORTC-NCIC trial. *Lancet Oncol.* **10**, 459–466 (2009).
6. R. Stupp *et al.*, Radiotherapy plus concomitant and adjuvant temozolomide for glioblastoma. *N. Engl. J. Med.* **352**, 987–996 (2005).
7. A. D. Fesnak, C. H. June, B. L. Levine, Engineered T cells: The promise and challenges of cancer immunotherapy. *Nat. Rev. Cancer* **16**, 566–581 (2016).
8. A. Ribas, J. D. Wolchok, Cancer immunotherapy using checkpoint blockade. *Science* **359**, 1350 (2018).
9. M. Lim, Y. Xia, C. Bettegowda, M. Weller, Current state of immunotherapy for glioblastoma. *Nat. Rev. Clin. Oncol.* **15**, 422–442 (2018).
10. J. H. Sampson, M. D. Gunn, P. E. Fecci, D. M. Ashley, Brain immunology and immunotherapy in brain tumours. *Nat. Rev. Cancer* **20**, 12–25 (2020).
11. D. Akhavan *et al.*, CAR T cells for brain tumors: Lessons learned and road ahead. *Immunol. Rev.* **290**, 60–84 (2019).
12. F. Wang *et al.*, Tumour sensitization via the extended intratumoural release of a STING agonist and camptothecin from a self-assembled hydrogel. *Nat. Biomed. Eng.* **4**, 1090–1101 (2020).
13. F. H. Wang *et al.*, Supramolecular prodrug hydrogelator as an immune booster for checkpoint blocker-based immunotherapy. *Sci. Adv.* **6**, eaaz8985 (2020).
14. D. Hambardzumyan, D. H. Gutmann, H. Kettenmann, The role of microglia and macrophages in glioma maintenance and progression. *Nat. Neurosci.* **19**, 20–27 (2016).
15. B. Badie, J. M. Schartner, Flow cytometric characterization of tumor-associated macrophages in experimental gliomas. *Neurosurgery* **46**, 957–961 (2000). Discussion 961–952.
16. S. Gholamin *et al.*, Disrupting the CD47-SIRPalpha anti-phagocytic axis by a humanized anti-CD47 antibody is an efficacious treatment for malignant pediatric brain tumors. *Sci. Transl. Med.* **9**, eaaf2968 (2017).
17. S. B. Willingham *et al.*, The CD47-signal regulatory protein alpha (SIRPa) interaction is a therapeutic target for human solid tumors. *Proc. Natl. Acad. Sci. U.S.A.* **109**, 6662–6667 (2012).
18. S. Gordon, Alternative activation of macrophages. *Nat. Rev. Immunol.* **3**, 23–35 (2003).
19. T. Calandra, T. Roger, Macrophage migration inhibitory factor: A regulator of innate immunity. *Nat. Rev. Immunol.* **3**, 791–800 (2003).
20. S. Jaiswal *et al.*, CD47 is upregulated on circulating hematopoietic stem cells and leukemia cells to avoid phagocytosis. *Cell* **138**, 271–285 (2009).
21. E. Sick *et al.*, CD47 update: A multifaceted actor in the tumour microenvironment of potential therapeutic interest. *Br. J. Pharmacol.* **167**, 1415–1430 (2012).
22. A. N. Barclay, T. K. van den Berg, The interaction between signal regulatory protein alpha (SIRP alpha) and CD47: Structure, function, and therapeutic target. *Annu. Rev. Immunol.* **32**, 25–50 (2014).
23. J. T. Sockolosky *et al.*, Durable antitumor responses to CD47 blockade require adaptive immune stimulation. *Proc. Natl. Acad. Sci. U.S.A.* **113**, E2646–2654 (2016).
24. D. Tseng *et al.*, Anti-CD47 antibody-mediated phagocytosis of cancer by macrophages primes an effective antitumor T-cell response. *Proc. Natl. Acad. Sci. U.S.A.* **110**, 11103–11108 (2013).
25. X. Liu *et al.*, CD47 blockade triggers T cell-mediated destruction of immunogenic tumors. *Nat. Med.* **21**, 1209–1215 (2015).
26. R. Advani *et al.*, CD47 blockade by Hu5F9-G4 and rituximab in non-hodgkin's lymphoma. *N. Engl. J. Med.* **379**, 1711–1721 (2018).
27. S. Gholamin *et al.*, Irradiation or temozolomide chemotherapy enhances anti-CD47 treatment of glioblastoma. *Innate. Immun.* **26**, 130–137 (2020).
28. C. A. von Roemeling *et al.*, Therapeutic modulation of phagocytosis in glioblastoma can activate both innate and adaptive antitumour immunity. *Nat. Commun.* **11**, 1508 (2020).
29. Q. Chen *et al.*, In situ sprayed bioresponsive immunotherapeutic gel for post-surgical cancer treatment. *Nat. Nanotechnol.* **14**, 89–97 (2019).
30. Y. Huang, Y. Ma, P. Gao, Z. Yao, Targeting CD47: The achievements and concerns of current studies on cancer immunotherapy. *J. Thorac. Dis.* **9**, E168–E174 (2017).
31. P. S. Petrova *et al.*, TTI-621 (SIRPalphaFc): A CD47-blocking innate immune checkpoint inhibitor with broad antitumor activity and minimal erythrocyte binding. *Clin. Cancer Res.* **23**, 1068–1079 (2017).
32. L. Gu, D. J. Mooney, Biomaterials and emerging anticancer therapeutics: Engineering the microenvironment. *Nat. Rev. Cancer* **16**, 56–66 (2016).
33. D. J. Irvine, E. L. Dane, Enhancing cancer immunotherapy with nanomedicine. *Nat. Rev. Immunol.* **20**, 321–334 (2020).
34. J. Ishihara *et al.*, Matrix-binding checkpoint immunotherapies enhance antitumor efficacy and reduce adverse events. *Sci. Transl. Med.* **9**, eaan0401 (2017).
35. J. Ishihara *et al.*, Targeted antibody and cytokine cancer immunotherapies through collagen affinity. *Sci. Transl. Med.* **11**, eaau3259 (2019).
36. L. Milling, Y. Zhang, D. J. Irvine, Delivering safer immunotherapies for cancer. *Adv. Drug. Deliv. Rev.* **114**, 79–101 (2017).

37. H. Wang, D. J. Mooney, Biomaterial-assisted targeted modulation of immune cells in cancer treatment. *Nat. Mater.* **17**, 761–772 (2018).
38. F. Wang, M. Porter, A. Konstantopoulos, P. Zhang, H. Cui, Preclinical development of drug delivery systems for paclitaxel-based cancer chemotherapy. *J. Control Release* **267**, 100–118 (2017).
39. M. De Palma, C. E. Lewis, Macrophage regulation of tumor responses to anticancer therapies. *Cancer Cell* **23**, 277–286 (2013).
40. Y. Zhao *et al.*, Chemotherapy-induced macrophage infiltration into tumors enhances nanographene-based photodynamic therapy. *Cancer Res.* **77**, 6021–6032 (2017).
41. D. Samanta *et al.*, Chemotherapy induces enrichment of CD47(+)/CD73(+)/PDL1(+) immune evasive triple-negative breast cancer cells. *Proc. Natl. Acad. Sci. U.S.A.* **115**, E1239–E1248 (2018).
42. R. W. Chakroun *et al.*, Fine-tuning the linear release rate of paclitaxel-bearing supramolecular filament hydrogels through molecular engineering. *ACS Nano.* **13**, 7780–7790 (2019).
43. L. L. Lock *et al.*, One-component supramolecular filament hydrogels as theranostic label-free magnetic resonance imaging agents. *ACS Nano.* **11**, 797–805 (2017).
44. F. Wang *et al.*, Supramolecular tubustecan hydrogel as chemotherapeutic carrier to improve tumor penetration and local treatment efficacy. *ACS Nano.* **14**, 10083–10094 (2020).
45. R. W. Chakroun *et al.*, Supramolecular design of unsymmetric reverse bolaamphiphiles for cell-sensitive hydrogel degradation and drug release. *Angew. Chem. Int. Ed. Engl.* **59**, 4434–4442 (2020).
46. H. Acar *et al.*, Self-assembling peptide-based building blocks in medical applications. *Adv. Drug. Deliver Rev.* **110**, 65–79 (2017).
47. V. A. Kumar *et al.*, Drug-triggered and cross-linked self-assembling nanofibrous hydrogels. *J. Am. Chem. Soc.* **137**, 4823–4830 (2015).
48. P. Schiapparelli *et al.*, Self-assembling and self-formulating prodrug hydrogelator extends survival in a glioblastoma resection and recurrence model. *J. Control Release* **319**, 311–321 (2020).
49. E. Sleep *et al.*, Injectable biomimetic liquid crystalline scaffolds enhance muscle stem cell transplantation. *Proc. Natl. Acad. Sci. U.S.A.* **114**, E7919–E7928 (2017).
50. C. Yan *et al.*, Injectable solid hydrogel: mechanism of shear-thinning and immediate recovery of injectable beta-hairpin peptide hydrogels. *Soft Matter.* **6**, 5143–5156 (2010).
51. L. E. R. O'Leary, J. A. Fallas, E. L. Bakota, M. K. Kang, J. D. Hartgerink, Multi-hierarchical self-assembly of a collagen mimetic peptide from triple helix to nanofibre and hydrogel. *Nat. Chem.* **3**, 821–828 (2011).
52. K. N. Sugahara *et al.*, Tissue-penetrating delivery of compounds and nanoparticles into tumors. *Cancer Cell* **16**, 510–520 (2009).
53. M. N. McCracken, A. C. Cha, I. L. Weissman, Molecular pathways: Activating T cells after cancer cell phagocytosis from blockade of CD47 "don't eat me" signals. *Clin. Cancer Res.* **21**, 3597–3601 (2015).
54. Q. Song *et al.*, Tumor microenvironment responsive nanogel for the combinatorial antitumor effect of chemotherapy and immunotherapy. *Nano. Lett.* **17**, 6366–6375 (2017).
55. L. W. Pfannenstiel, S. S. K. Lam, L. A. Emens, E. M. Jaffee, T. D. Armstrong, Paclitaxel enhances early dendritic cell maturation and function through TLR4 signaling in mice. *Cell Immunol.* **263**, 79–87 (2010).
56. H. Su, W. Zhang, H. Wang, F. Wang, H. Cui, Paclitaxel-promoted supramolecular polymerization of peptide conjugates. *J. Am. Chem. Soc.* **141**, 11997–12004 (2019).
57. J. Bianco *et al.*, Novel model of orthotopic U-87 MG glioblastoma resection in athymic nude mice. *J. Neurosci. Methods* **284**, 96–102 (2017).
58. D. Mathios *et al.*, Anti-PD-1 antitumor immunity is enhanced by local and abrogated by systemic chemotherapy in GBM. *Sci. Transl. Med.* **8**, 370ra180 (2016).